2-1-2009

Nonrigid registration of three-dimensional ultrasound and magnetic resonance images of the carotid arteries

Nuwan D Nanayakkara

Bernard Chiu

Abbas Samani

J David Spence

Jagath Samarabandu

See next page for additional authors

Nonrigid registration of three-dimensional ultrasound and magnetic resonance images of the carotid arteries

Nuwan D. Nanayakkara[a] and Bernard Chiu
Imaging Research Laboratories, Robarts Research Institute, London, Ontario N6A 5K8, Canada and Graduate Program in Biomedical Engineering, The University of Western Ontario, London, Ontario N6A 3K7, Canada

Abbas Samani
Department of Medical Biophysics and Department of Electrical and Computer Engineering, The University of Western Ontario, London, Ontario N6A 3K7, Canada

J. David Spence
Department of Neurology and Department of Clinical Pharmacology, The University of Western Ontario, London, Ontario N6A 3K7, Canada and Stroke Prevention and Atherosclerosis Research Centre, Robarts Research Institute, London, Ontario N6A 5K8, Canada

Jagath Samarabandu
Department of Electrical and Computer Engineering, The University of Western Ontario, London, Ontario N6A 3K7, Canada

Grace Parraga
Imaging Research Laboratories, Robarts Research Institute, London, Ontario N6A 5K8, Canada and Department of Medical Biophysics, The University of Western Ontario, London, Ontario N6A 3K7, Canada

Aaron Fenster[b]
Imaging Research Laboratories, Robarts Research Institute, London, Ontario N6A 5K8, Canada and Graduate Program in Biomedical Engineering, The University of Western Ontario, London, Ontario N6A 3K7, Canada

(Received 30 May 2008; revised 1 December 2008; accepted for publication 4 December 2008; published 12 January 2009)

Atherosclerosis at the carotid bifurcation can result in cerebral emboli, which in turn can block the blood supply to the brain causing ischemic strokes. Noninvasive imaging tools that better characterize arterial wall, and atherosclerotic plaque structure and composition may help to determine the factors which lead to the development of unstable lesions, and identify patients at risk of plaque disruption and stroke. Carotid magnetic resonance (MR) imaging allows for the characterization of carotid vessel wall and plaque composition, the characterization of normal and pathological arterial wall, the quantification of plaque size, and the detection of plaque integrity. On the other hand, various ultrasound (US) measurements have also been used to quantify atherosclerosis, carotid stenosis, intima-media thickness, total plaque volume, total plaque area, and vessel wall volume. Combining the complementary information provided by 3D MR and US carotid images may lead to a better understanding of the underlying compositional and textural factors that define plaque and wall vulnerability, which may lead to better and more effective stroke prevention strategies and patient management. Combining these images requires nonrigid registration to correct the nonlinear misalignments caused by relative twisting and bending in the neck due to different head positions during the two image acquisition sessions. The high degree of freedom and large number of parameters associated with existing nonrigid image registration methods causes several problems including unnatural plaque morphology alteration, high computational complexity, and low reliability. Thus, a "twisting and bending" model was used with only six parameters to model the normal movement of the neck for nonrigid registration. The registration technique was evaluated using 3D US and MR carotid images at two field strengths, 1.5 and 3.0 T, of the same subject acquired on the same day. The mean registration error between the segmented carotid artery wall boundaries in the target US image and the registered MR images was calculated using a distance-based error metric after applying a "twisting and bending" model based nonrigid registration algorithm. An average registration error of 1.4 ± 0.3 mm was obtained for 1.5 T MR and 1.5 ± 0.4 mm for 3.0 T MR,

when registered with 3D US images using the nonrigid registration technique presented in this paper. Visual inspection of segmented vessel surfaces also showed a substantial improvement of alignment with this nonrigid registration technique compared to rigid registration. © *2009 American Association of Physicists in Medicine.* [DOI: 10.1118/1.3056458]

Key words: registration, three-dimensional ultrasound, magnetic resonance (MR), carotid plaque, atheroscleroses

I. INTRODUCTION

Stroke is a leading cause of death and long-term disability in North America.[1,2] Approximately 85% of strokes are ischemic, and these are believed to result because of blockage of a cerebral artery or arteriole. Atherosclerosis at the carotid bifurcation is a major cause of occlusion or cerebral emboli.[3] A number of studies have shown that the majority of patients with highly stenotic, atherosclerotic carotid plaque remain asymptomatic,[4,5] whereas patients with atherosclerotic plaques that are vulnerable to disruption, fracture, or fissuring can be at higher risk for embolization, occlusion, and consequent ischemic strokes.[6–8] The development of noninvasive imaging tools[9–13] that better characterize arterial wall, and atherosclerotic plaque structure and composition may help to determine the factors which lead to the development of unstable lesions, and identify patients at risk of plaque disruption and stroke. Furthermore, a better understanding of dynamic characteristics of tissue strain and wall shear stress in the presence of different plaque components may also lead to better predictive models for atherosclerotic lesion disruption.[14,15]

As an emerging research technique, multicontrast weighted carotid magnetic resonance (MR) imaging allows for the characterization of carotid vessel wall and plaque composition,[13,16] as well as the characterization of normal and pathological arterial wall,[9] the quantification of plaque size,[17] and the detection of plaque integrity.[18,19] MR angiography (MRA) and high-resolution black-blood imaging of the vessel wall can be combined to evaluate the severity of stenotic lesions with their spatial distributions, and composition of the plaque for risk assessment and selection of treatment options.[20,21] On the other hand, various ultrasound (US) measurements have also been used to quantify atherosclerosis both in research and clinical settings.[22] Doppler US is also used in the clinical setting to assess the severity of carotid stenosis, which is a well-established stroke risk factor,[23] by measuring peak systolic and peak diastolic velocity or their ratio.[24] The one-dimensional US measurement of intima-media thickness (IMT) is also widely used in research for assessment of cardiovascular risk factors.[25,26] Recent developments in 3D US imaging have allowed for the measurement of total plaque volume,[11,27,28] total plaque area,[29] and 3D US vessel wall volume.[30,31] In addition, the ability of US to identify different carotid plaque components has also been investigated using carotid endarterectomy specimens for validation.[10,12]

Combining the complementary information provided by 3D MR and US carotid images may lead to a better understanding of the underlying compositional and textural factors that define plaque and wall vulnerability,[15] which may lead to better and more effective stroke prevention strategies and patient management.[32] Furthermore, it may be advantageous to combine noninvasive MR plaque composition information with 3D US images, since it would provide a tool for *in vivo* validation of US plaque characterization techniques. However, the patient's head position is different in each image acquisition session causing relative bending and twisting of the carotid artery in 3D images. Thus, the image data acquired using the two imaging modalities would have relative nonlinear deformations between them, and these misalignments must be corrected by nonrigid image registration to allow proper registration of images acquired using these two modalities.[15,33]

A few reports of carotid image registrations have appeared in the literature. Slomka *et al.* reported a 3D registration algorithm for carotid images, in which they used mutual information (MI) for rigid registration of 3D MRA images with power Doppler US (and indirectly with 3D US).[34] Fei *et al.*[35] reported an automatic rigid registration algorithm for multiple contrast weighted MR images of carotid vessels. Chan *et al.*[15] reported the first nonrigid registration algorithm for 3D carotid image registration, in which they applied an unconstrained thin-plate-spline based deformable registration to carotid MR and 3D US images of *ex vivo* carotid artery samples and observed mean registration errors of about 1 mm. The authors previously presented a single modality (3D US) nonrigid registration algorithm for the registration of 3D US carotid images obtained at two different imaging sessions using a "twisting and bending" model to correct misalignments between images due to the movements of the neck.[36] The authors successfully used the twisting and bending model to keep the deformations in the images within the natural neck movements during the registration to avoid any possible unnatural warping of the image that can mask the actual changes in the plaque structure.

Accordingly, this paper presents a method for multimodality nonrigid registration of 3D US carotid images with 3D MR images of the same subject, which extends the twisting and bending model-based 3D US to US nonrigid registration of carotid images[36] that the authors previously developed. Here MI[37,38] is used as the image similarity measure since it has been used successfully in US–MR image registration.[39] The authors applied the proposed algorithm to 3D carotid US and MR images obtained from patients with carotid total plaque area >0.5 cm^2 and evaluated the registration accuracy using a distance based error metric[36] between segmented vessel surfaces.

II. MATERIALS AND METHODS

II.A. Nonrigid registration

In registration, any point, (x,y,z) in a 3D MR image of the carotid artery (*source*) relates to a point in the reference 3D US image of the same region (*target*), which is acquired separately, using the optimal transformation,

$$\mathbf{T}:(x,y,z) \mapsto (x',y',z'). \tag{1}$$

In general, different head positions in different image acquisition sessions cause nonlinear deformations between the images, so that rigid transformation alone is not sufficient for registration. Therefore, a combined transformation, $\mathbf{T}$, which consists of a rigid transformation for coarse alignment and a nonrigid transformation for fine alignment, is required,

$$\mathbf{T}(x,y,z) = \mathbf{T}_{\text{nonrigid}}[\mathbf{T}_{\text{rigid}}(x,y,z)]. \tag{2}$$

II.A.1. Rigid transformation

Rigid transformation, in 3D, has six degrees of freedom, describing three rotations, $\theta_x, \theta_y, \theta_z$, and the three translations, t_x, t_y, t_z, and is defined in the following.

$$\mathbf{T}_{\text{rigid}}(x,y,z) = \mathbf{R}_{\theta_x,\theta_y,\theta_z}\begin{pmatrix} x \\ y \\ z \end{pmatrix} + \begin{pmatrix} t_x \\ t_y \\ t_z \end{pmatrix}, \tag{3}$$

where $\mathbf{R}_{\theta_x,\theta_y,\theta_z}$ is the standard rotation matrix for angles θ_x, θ_y, and θ_z.[40]

II.A.2. Nonrigid transformation: Twisting and bending model

In previous work, the authors modeled the movement of the neck using a twisting and bending model with only six parameters for a nonrigid transformation to be used for carotid 3D US image registration,[36] as summarized in the following. The twisting and bending model limits deformations to the natural neck movements only, avoiding unnatural changes to plaque morphology during the registration. The authors' nonrigid transformation consists of two parts, twisting and bending,

$$\mathbf{T}_{\text{nonrigid}}(x,y,z) = \mathbf{T}_{\text{bend}}[\mathbf{T}_{\text{twist}}(x,y,z)]. \tag{4}$$

The twisting model assumes that the 3D carotid image is a part of a homogeneous cylindrical shaft, which is clamped at the bottom plane of the z axis (at $z=0$), as shown in Fig. 1(a). The center of the model, the "twist–bend center" defined by three parameters (X_c,Y_c,Z_c), does not move during the deformation. The twisting is defined by one parameter, Q, where $|Q|$ represents the magnitude of the vector torque, $\mathbf{Q}$, and $Q>0$ describes clockwise and $Q<0$ describes counterclockwise twisting. Any plane perpendicular to the twisting axis is not distorted under the homogeneous cylindrical shaft assumptions.[41] Each plane normal to the z axis rotates around the axis with a different angle, $\phi(z)$, as shown in Fig. 1(a) and the transformation for twisting, $\mathbf{T}_{\text{twist}}(x,y,z)$, is then given by

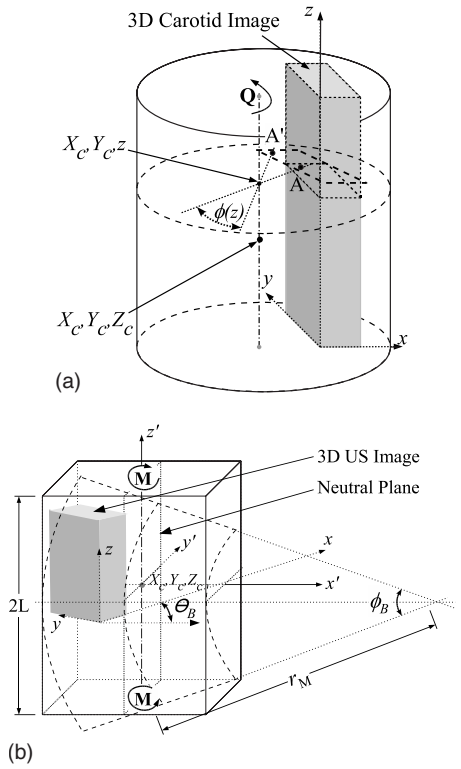

FIG. 1. "Twisting and bending" model. (a) The twisting model assumes that the 3D carotid image (shown as the gray block) is a part of a cylindrical shaft. The model parameters (X_c,Y_c,Z_c) defines the "twist–bend center," which does not move during the deformation, where $\mathbf{Q}$ is the twisting torque and $\phi(z)$ is the twisting angle at the plane normal to the z axis passing through (X_c,Y_c,z). (b) The bending model assumes that 3D carotid image (shown as the gray block) is a part of a rectangular homogeneous shaft with the center axis going through the twist–bend center (X_c,Y_c,Z_c). A new coordinate system, (x',y',z') is defined at the twist–bend center with the x' axis defined in the "bending direction" at an angle θ_B to the x axis. Then, the bending is defined in (x',y',z') coordinate system, where the length of the neutral plane does not change during bending, and bending moment, $\mathbf{M}$ creates a bending angle θ_B due to the curvature $1/r_M$.

$$\mathbf{T}_{\text{twist}}(x,y,z) = \begin{pmatrix} t_{11} & t_{12} & 0 \\ t_{21} & t_{22} & 0 \\ 0 & 0 & 1 \end{pmatrix}\begin{pmatrix} x-X_c \\ y-Y_c \\ z-Z_c \end{pmatrix} + \begin{pmatrix} X_c \\ Y_c \\ Z_c \end{pmatrix}, \tag{5}$$

where $t_{11}=\cos[\phi(z)]$, $t_{12}=-\sin[\phi(z)]$, $t_{21}=\sin[\phi(z)]$, $t_{22}=\cos[\phi(z)]$, $\phi(z)=(\pi/4L)Qz$.

The bending was modeled assuming a pure bending condition under equal and opposite bending moments, $\mathbf{M}$, acting at the two ends of the z axis.[41] The 3D carotid image is assumed to be a part of a rectangular block for the bending model, with length, $2L$ in the z direction and centered at the twist–bend center (X_c,Y_c,Z_c) as shown in Fig. 1(b), where L is the length of the 3D carotid image along the z axis. The bending model has two parameters defining the two components, M_x and M_y, of the bending moment $\mathbf{M}$, in the two directions x and y, respectively. The component of the bending moment along the z axis is always zero since the bending moment, $\mathbf{M}$, is perpendicular to the z axis. Thus, the direction of the bending is defined by the angle to the x axis, θ_B, as defined by

$$\theta_B = \tan^{-1}\left(\frac{M_y}{M_x}\right). \quad (6)$$

First, a new coordinate system, (x',y',z') is defined at the twist–bend center, which is rotated around the z' axis by the angle θ_B to make the bending always defined in the direction of the x' axis. Subsequently, the transformation for bending in (x',y',z') coordinate system is given by Eq. (7) as shown in Fig. 1(b),

$$\mathbf{T}'_{\text{bend}}(x',y',z') = \begin{pmatrix} r_M - (r_M - x')\cos\left(\frac{z'}{r_M}\right) \\ y' \\ (r_M - x')\sin\left(\frac{z'}{r_M}\right) \end{pmatrix}, \quad (7)$$

where curvature $1/r_M = (\pi/4L)|\mathbf{M}|$ and $|\mathbf{M}| = \sqrt{M_x^2 + M_y^2}$.

Finally, the transformation, $\mathbf{T}'_{\text{bend}}(x',y',z')$ is rotated by $-\theta_B$ and translated by $(-X_c,-Y_c,-Z_c)$ to define $\mathbf{T}_{\text{bend}}(x,y,z)$ in the original coordinate system.

II.A.3. Registration process

The registration process finds the best transformation, $\mathbf{T}$, that maximizes the normalized mutual information (NMI) between the target image I_t and the transformed source image I_s^T. The corresponding values for all the registration parameters, three rotations $(\theta_x,\theta_y,\theta_z)$, three translations (t_x,t_y,t_z), twisting torque $(|\mathbf{Q}|)$, bending moments (M_x,M_y), and twist–bend center (X_c,Y_c,Z_c) are required to be found using an optimization process. The $\text{NMI}(I_t,I_s^T)$ is defined using image entropies as given in Eq. (8), which is less sensitive to changes in image overlap.[42]

$$\text{NMI}(I_t,I_s^T) = \frac{H(I_t) + H(I_s^T)}{H(I_t,I_s^T)}, \quad (8)$$

where $H(I_t)$ and $H(I_s^T)$ denote marginal entropies of corresponding images, and $H(I_t,I_s^T)$ defines their joint entropy.[43] The calculations were based on the method of Mattes *et al.*,[44,45] where the probability density distribution is estimated using Parzen histograms. This method was largely insensitive to the size of the histogram.[44] We set the histogram to 64 bins for the experiments in this paper. The Powell optimizer[46] was used for numerical optimization to find the best set of registration parameters that maximize the NMI. Linear interpolation was employed in registration when transforming the source image, as it provided a sufficiently smooth optimization within a reasonable computational time.[47] The registration framework in the Insight Toolkit[48] was used for implementing the authors' algorithm.

II.A.4. Preprocessing

A median filter with a kernel size of $5\times5\times5$ voxels on the 3D US carotid images was used to reduce the effect of speckle as a preprocessing step. Speckle is an integral part of US images and conveys useful information to the radiologist, but causes problems in registration.[49] In addition, the interference of other anatomical structures in carotid 3D US images may cause errors in registration. Therefore, the region outside of the carotid artery and its vicinity was masked out, keeping only a region about half a diameter of the common carotid from the outer carotid boundary. To define a conical region of interest (ROI), two circles were defined at the top and the bottom planes perpendicular to the z axis, enclosing the carotid artery (or two arterial sections on the top plane) and the surrounding area up to a length approximately equal to a half a diameter of the common carotid. To define the circles, the user chose two points on the perimeter of each circle at two ends of an imaginary line passing through the center. Then, the cone-shaped ROI was defined using those two circles as cross sections, and the volume outside was masked out as shown in Fig. 2. MR images contain carotid arteries of both sides of the neck together with other anatomical structures. Therefore, the authors used the ROI for registration to select only the corresponding carotid artery (left and right separately) and its surrounding area using the same procedure as for the 3D US images, as shown in Fig. 2(c).

II.A.5. Registration initialization

To initialize the registration, the user first selected the carotid bifurcation in both target and source images. Then the source image was approximately aligned with the target image by aligning the user-selected bifurcations (BFs) [as shown in Fig. 3(a)] by introducing an initial translation. It has been shown that the carotid bifurcation can be located in 3D US images with a standard deviation of 0.56 mm.[27] In addition, the initial rotation angles $(\alpha_x,\alpha_y,\alpha_z)$ were calculated using the BF points and another three user-selected points: center of the common carotid, c, at the bottom and centers through internal, i, and external, e, carotid arteries at the transverse plane of the bifurcation as shown in Fig. 3(a). Since this initial coarse alignment was allowed to change during the registration, it was assumed that the variations in the choice of the initialization were relatively insignificant to the final registration results.

II.B. Evaluation of accuracy

II.B.1. Image acquisition

Two 3D US images of the left and right carotids, and two MR images of the neck at field strengths, 1.5 and 3.0 T, were acquired from each subject of a patient population with carotid total plaque area >0.5 cm^2, who were recruited from the Premature Atherosclerosis Clinic and The Stroke Prevention Clinic at University Hospital, London Health Sciences Center, London, Canada. Images were selected from six subjects for a total of 12 separate 3D US images of left and right carotids and corresponding 1.5 and 3.0 T MR images to evaluate the proposed nonrigid registration algorithm. Two MR field strengths were used to study the effect of signal-to-noise (SNR) and contrast-to-noise (CNR) ratios at different field strengths on US–MR nonrigid registration accuracy.

All subjects were scanned at 1.5 and 3.0 T with GE EXCITE whole-body MR systems, with identical pulse sequences and identical custom-built six-element carotid-

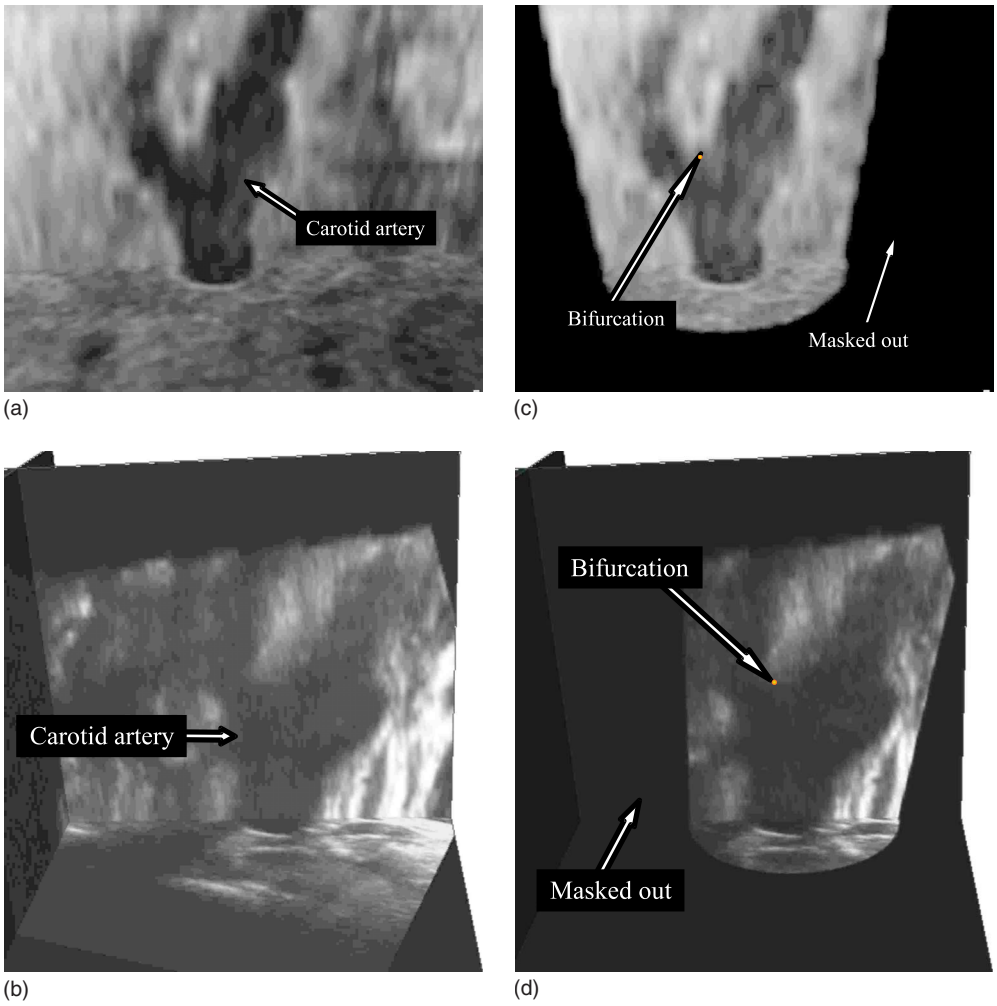

FIG. 2. Images showing preprocessing of 3D MR and US images for registration. The 3D MR and US images have been sliced to show longitudinal views of the branches of the carotid artery: (a) MR, (b) US, and (c) and (d) corresponding views after masking. The user-selected bifurcation is also shown.

bifurcation-optimized receive-only phased-array coils. Both receive-only coils were geometrically and electronically identical, but with one tuned for use at 1.5 T and the other for use at 3.0 T. For both scanners, a specialized foam head holder was also used to reduce positioning variability and to provide comfortable but secure immobilization of each subject's head. The time frame between MRI scanning sessions at each field strength was approximately 2 h. Multiple MR sequences were acquired and the total acquisition time for all sequences was approximately 60 min. At both 3.0 and 1.5 T, a set of 100, 2-mm-thick axial 2D time-of-flight slices were acquired in 4 min to identify the superior–inferior level of the flow dividers on each side. A localized shim was performed prior to each of the remaining sequences to ensure good performance of fat saturation pulses. The remaining series consisted of a multislice 2D black-blood acquisition, with T1-weighted (T1w) contrast, using double inversion recovery (DIR with 180° pulse). Parameters for the T1w scans analyzed in this study and acquired at 1.5 and 3.0 T are provided in Table I. All images following the localizer were acquired with 0.5 mm in-plane resolution, 2 mm slice thickness, and fat saturation. Subject motion was monitored by examining odd-to-even slice misregistration, and image data sets with substantial motion were not used in the study. All postlocalizer series were planned with slices centered in the superior–inferior direction at a point 5 mm superior to the flow divider of the index bifurcation. The T1w sequences were acquired with 16 contiguous 2-mm-thick slices covering 32 mm in the head-foot axis. In this paper, T1w scans were chosen for analysis because of previously published analysis that showed that blood flow suppression was best achieved using the single slice DIR technique widely used for MR carotid plaque imaging.[50,51]

Carotid US scans were performed at the Imaging Research Laboratories, Robarts Research Institute, using an HDI 5000 US machine (Philips/ATL). An L12-5 probe with a central frequency of 8.5 MHz was used in the composite imaging (SonoCT) mode. The transducer was attached to a motorized linear mechanical mover, oriented and translated along the neck for about 4 cm (in ≈8 s) approximately centered on the bifurcation while capturing 2D US slices at 30 slices/s to produce 3D US images with voxel sizes $\approx 0.1 \times 0.1 \times 0.15$ mm using a 3D imaging system developed in the authors laboratory.[11,28]

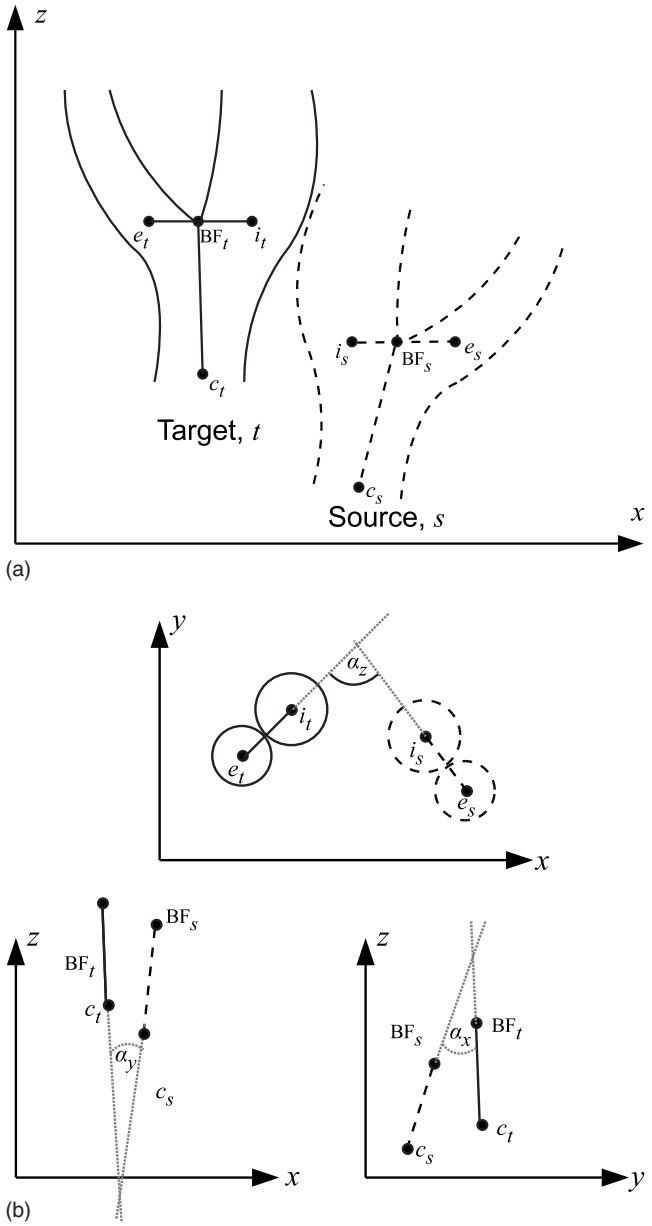

FIG. 3. Registration initialization: (a) User-defined points, bifurcation points (BF), center of the common carotid, *c*, at the bottom and centers of internal, *i*, and external, *e*, carotid arteries at the transverse plane through the bifurcation, and (b) initial rotation angles $(\alpha_x, \alpha_y, \alpha_z)$ on the three orthogonal planes.

TABLE I. Magnetic resonance imaging parameters for T1-weighted double inversion recovery scans at 1.5 and 3.0 T.

Acquisition parameter	1.5 T	3.0 T
Echo time, TE (ms)	12	11.4
Recovery time, TR	1RR	1RR
Receiver bandwidth, RBW (kHz)	41.67	41.67
Field of view, FOV (cm)	11	11
Thickness (mm)	2	2
Matrix	224×224	224×224
Number of excitations, NEX	3	3
Scan time (min)	8:48	8:48
Fat saturation	Yes	Yes
Spacing overlap	0	0
Number of slices	16	16
Pulse sequence	FSE	FSE

II.B.2. Registration error metric

The authors previously used the carotid artery media-adventitia boundary to calculate the registration error for intramodality 3D carotid US image registration.[36] Thus, a similar approach was used to calculate the registration error in multimodality 3D US and MR carotid image registration. However, the media-adventitia boundary is not clearly visible in MR carotid images and the segmented boundary corresponds to the adventitia-tissue boundary.[52] Therefore, the segmented media-adventitia boundary in US images was expanded by the average adventitia thickness to make it correspond to the segmented adventitia-tissue boundary in MR images. Wong *et al.*[53] reported that the average adventitia thickness in US images is 0.5 ± 0.1 mm, and thus the authors expanded the segmented media-adventitia boundary in US images by 0.5 mm before the distance-based registration error calculation described in the following.

The carotid artery outer wall boundaries in the target 3D US and registered MR images were manually segmented by a trained observer for evaluation of the proposed registration algorithm. Although the algorithm used 3D US and MR images of the whole vessel for registration, the carotid artery surface was examined in three sections (internal, external, and common carotid) to estimate the registration error in each branch. In each carotid surface section, k ($k=1$:common, 2:internal, 3:external) the registration error was calculated as the distance, $d_{i,j,k}$ between corresponding points, $(x^t_{i,j,k}, y^t_{i,j,k})$ on the target and $(x^r_{i,j,k}, y^r_{i,j,k})$ on the registered surfaces in each plane, j $(j=1,2,\ldots,N_k)$ normal to the *z axis* at every 1 mm interval as shown in Fig. 4 and defined in the following:

$$d_{i,j,k} = \left\| (x^t_{i,j,k}, y^t_{i,j,k}) - (x^r_{i,j,k}, y^r_{i,j,k}) \right\|. \quad (9)$$

The corresponding points were defined by projecting radial lines, i $(i=1,2,\ldots,90)$, from the center of each contour to the corresponding surface at the same angle at 4° intervals, as described in the evaluation of nonrigid registration of 3D

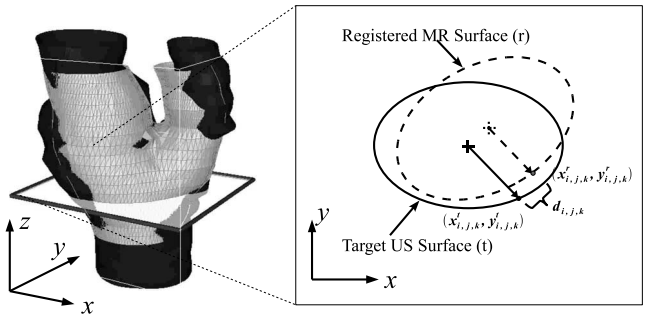

FIG. 4. Registration error calculation using the distance between corresponding points, on the target $(x^t_{i,j,k}, y^t_{i,j,k})$ and registered $(x^r_{i,j,k}, y^r_{i,j,k})$ surfaces at the direction, i, on each plane, j, normal to z axes at every 1 mm in carotid section, k.

US–US carotid images.[36] The resulting 3D distributions of registration error values were also used for better visualizing and analysis of the registration accuracy by mapping the color-coded distance $d_{i,j,k}$ onto the segmented carotid surfaces.

The mean registration error (MRE_k) was defined for each carotid section, k, for individual image sets as described in the following:

$$MRE_k = \frac{1}{90N_k}\left(\sum_{j=1}^{N_k}\sum_{i=1}^{90} d_{i,j,k}\right). \quad (10)$$

The mean registration error (MRE) was also calculated for the whole vessel, to express the registration error by a single numerical value as given in the following:

$$MRE = \frac{1}{90\Sigma_{k=1}^{3}N_k}\left(\sum_{k=1}^{3}\sum_{j=1}^{N_k}\sum_{i=1}^{90} d_{i,j,k}\right). \quad (11)$$

The maximum registration errors ($MAXE_k$) were also calculated for each carotid section, k, for individual image sets as described in the following:

$$MAXE_k = \max_{j\in[1,N_k]}\left(\max_{i\in[1,90]} d_{i,j,k}\right). \quad (12)$$

The registration error $d_{i,j,k}$ between the segmented vessel surfaces in the target image and the registered image includes the error due to the variability in surface segmentations as well. To reduce the effect of the segmentation errors in registration error calculations, the mean surface of five repeated segmentations of the expert user was used, with at least 5 days between the segmentation operations as was done in the US–US registration error calculations.[36]

II.B.3. Nonrigid registration accuracy

MR images were registered at field strengths of 1.5 and 3.0 T separately with corresponding 3D US images using the authors' twisting and bending model-based nonrigid registration algorithm. The MRE_k was calculated separately for each carotid section, k, as well as the MRE for the whole vessel (all three sections together) in all the samples. The authors also calculated the average MRE_k and MRE and the standard deviation of all 12 carotid vessels using the values of MRE_k and MRE of individual samples.

II.B.4. Comparison of rigid and nonrigid registration results

The registration error calculations as described earlier in Sec. II B 3 for the rigid registration were repeated and the errors were compared to those of nonrigid registration to analyze the capabilities of the nonrigid registration method in improving the registration accuracy. The significance of the improvement was analyzed statistically using *paired t-tests* separately for each carotid section, as well as for the whole vessel together. In addition, the $MAXE_k$ was calculated separately for each carotid section, k, for all rigid and nonrigid registrations to examine the ability of nonrigid registration in correcting large localized errors of rigid registration.

II.B.5. Registration error as a function of the distance from carotid bifurcation

Distribution of registration error along the carotid artery is an important factor in evaluating the effectiveness of the registration results. For a example, since most of the carotid plaque occurs around the bifurcation, a low registration error close to the bifurcation is preferable. To study this, the authors calculated the average registration error on each plane perpendicular to the z axis as a function of the distance, s, from the carotid bifurcation to that plane, in each carotid section, k, for both field strengths as described in Eq. (13). The distance s was defined by the distance along the z axis from the user-defined carotid bifurcation,

$$MRE_{s,k} = \frac{1}{90}\sum_{i=1}^{90} d_{i,s,k}. \quad (13)$$

II.B.6. Comparison of US–MR registration errors at two MR field strengths

Recent studies have shown that SNR and CNR ratios were higher in carotid MR images acquired at 3.0 T as compared to 1.5 T.[51] The authors studied the effect of these changes on US–MR carotid nonrigid registration by comparing the registration errors at the two field strengths using a *paired t-test* at each carotid section, k, as well as all three carotid branches together for all image samples.

III. RESULTS

The tests were performed on a personal computer running Windows 2000 OS with a Pentium 4, 2.4 GHz processor, and 1 gbytes of RAM. The registration program was implemented with ITK[48] without optimizing it for processing time. The registration time after initialization ranged from 10 to 40 min for one pair of images for those reported in this paper.

III.A. Nonrigid registration accuracy

The twisting and bending model-based nonrigid registration algorithm was applied to register each of 12 US images with corresponding 1.5 and 3.0 T MR images separately. Figure 5 shows a sample result, where Figs. 5(a) and 5(b) show the segmented vessel boundaries for 1.5 and 3.0 T, respectively, while Figs. 5(c) and 5(d) show the corresponding distance-based registration errors calculated and mapped onto the carotid surfaces on MR images. Table II shows the registration errors of twisting and bending model-based, intrasubject, nonrigid registrations of US with 1.5 and 3.0 T MR separately for 3D images of carotid artery for all data sets, as well as the average values for all the samples. It is important to note that the internal and common carotid arteries showed a lower mean registration error than the corre-

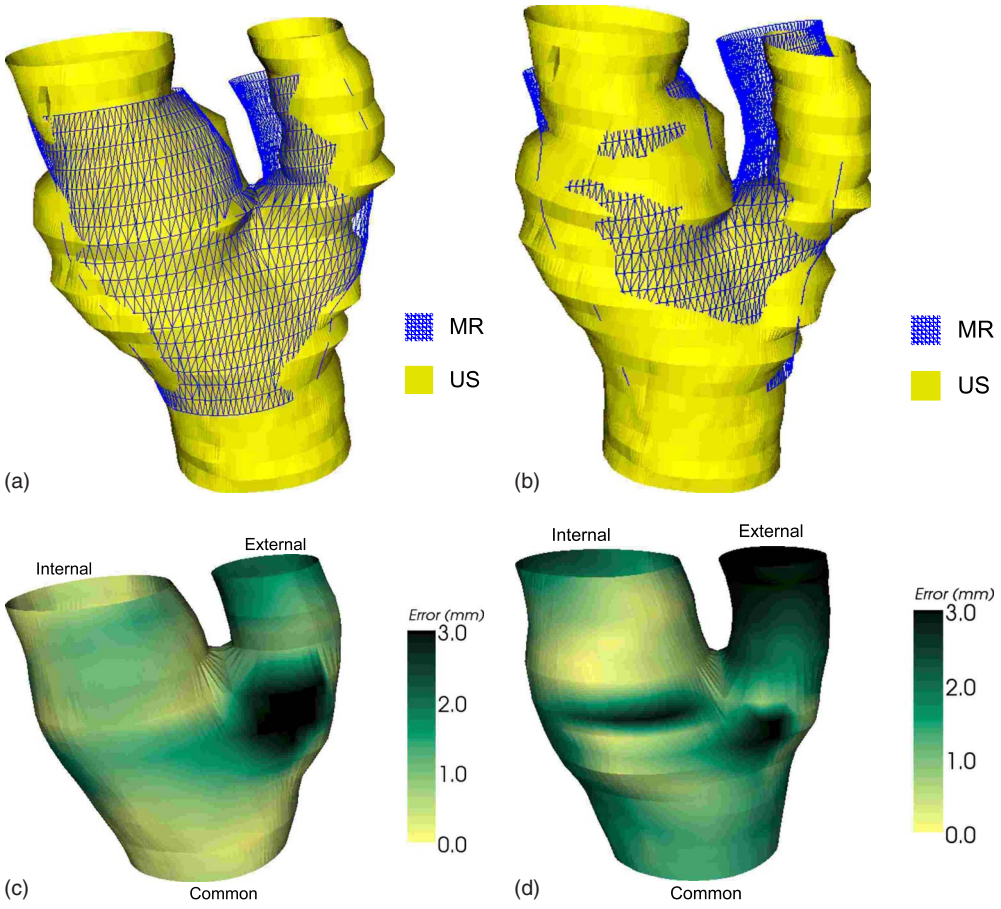

FIG. 5. Examples of registration results showing vessel boundaries after twisting and bending model-based nonrigid registration using: (a) 3D US with 1.5 T MR, (b) 3D US with 3.0 T MR. The color-coded registration errors, $d_{i,j,k}$(mm), have been mapped on the registered MR surfaces using: (c) 3D US with 1.5 T MR and (d) 3D US with 3.0 T MR.

TABLE II. Distance-based mean registration error (MRE_k) for twisting and bending model-based nonrigid registration of US with 1.5 T MR and US with 3.0 T MR for the $k=1$: common, 2: internal, and 3: external carotid artery segments, as well as MRE for the whole vessel. Note that the 3D images of the whole vessel here used in the registration procedure. The last row shows the overall mean (and standard deviation in parentheses) for all of the image sets.

	Mean registration error, MRE_k (mm)						MRE (mm)	
	$k=1$: Common		$k=2$: Internal		$k=3$: External		Whole vessel	
	1.5 T	3.0 T	1.5 T	3.0 T	1.5 T	3.0 T	1.5 T	3.0 T
Subject1-L	0.8	1.5	0.7	1.0	1.4	2.7	0.9	1.7
Subject1-R	0.9	1.0	2.5	1.1	0.8	3.6	1.2	1.6
Subject2-L	1.1	3.0	1.5	1.3	2.3	2.2	1.5	2.3
Subject2-R	1.0	0.9	1.3	1.2	1.2	1.7	1.1	1.1
Subject3-L	2.1	1.9	1.0	1.3	0.8	0.4	1.4	1.4
Subject3-R	2.5	2.8	1.8	0.8	1.7	1.1	2.0	1.7
Subject4-L	1.0	0.7	0.7	2.0	1.5	1.1	1.1	1.2
Subject4-R	2.1	2.1	1.0	1.2	1.2	1.6	1.5	1.7
Subject5-L	1.5	1.3	1.4	1.1	2.0	1.6	1.6	1.3
Subject5-R	1.2	0.7	2.4	1.4	0.6	1.3	1.4	1.0
Subject6-L	1.5	1.1	0.9	0.8	3.2	0.8	1.8	0.9
Subject6-R	0.8	1.3	1.8	1.1	2.3	2.9	1.5	1.6
Overall mean	1.4	1.5	1.4	1.2	1.6	1.8	1.4	1.5
(s.d.)	(0.6)	(0.8)	(0.6)	(0.3)	(0.8)	(0.9)	(0.3)	(0.4)

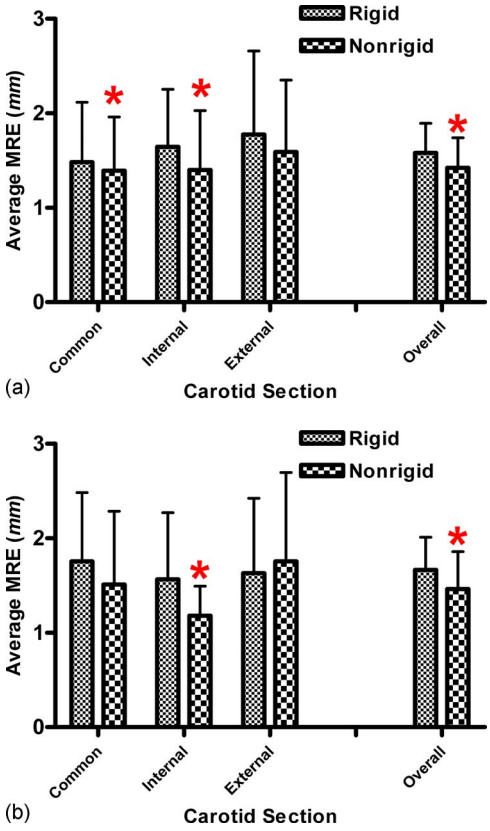

FIG. 6. Average MRE_k for different carotid sections, k, and MRE for whole vessel of all samples for intrasubject rigid and twisting and bending model-based nonrigid registration of (a) 3D US with 1.5 T MR and (b) 3D US with 3.0 T MR images of carotid artery, where an asterisk indicates statistically significant (*paired t-test*, $P<0.05$) reduction in registration error.

sponding external artery for both 1.5 and 3.0 T MR images. This is an important result, since carotid plaques are found in the common and internal carotid arteries.

III.B. Comparison of rigid and nonrigid registration results

Each of the 12 US images was registered with corresponding 1.5 and 3.0 T MR images using only rigid registration to analyze the improvement in registration accuracy for twisting and bending model-based nonrigid registration. Figure 6 shows the average MRE_k of all image samples for different carotid sections, and average MRE for the whole vessel. Results of *paired t-tests* ($\alpha=0.05$, $1-\beta=0.8$, $P<0.05$) in Table III showed that the registration error decreased significantly for the whole vessel as well as in the internal carotid artery for nonrigid registration of US images with MR images of both field strengths, but the change was not significant in the external carotid artery. Registration error in the common carotid artery showed a small but significant improvement over rigid registration for 1.5 T MR, while the change in registration error is not significant for 3.0 T MR. The normal distribution of all MRE_k and MRE values was tested using the Kolmogorov–Smirnov normality test.[54]

The maximum registration error, $MAXE_k$, was also calculated for each carotid section separately for rigid and nonrigid registration of US carotid images with 1.5 and 3.0 T MR images and results are shown in Table IV. These results indicated that twisting and bending model-based nonrigid registration was able to reduce the maximum registration error in 52 of the 72 cases tested.

III.C. Registration error as a function of the distance from carotid bifurcation

Figure 7 shows the average $MRE_{s,k}$ of planes perpendicular to the z axis for rigid registration as well as twisting and bending model-based nonrigid registration of 3D US with 1.5 and 3.0 T MR images separately. For all cases, registration error increased on planes away from the bifurcation, and could be justified since the registration process was started by aligning the bifurcations of target and source images. Therefore, a high registration accuracy was observed around the carotid bifurcation. This result is important since carotid plaque normally develops near the carotid bifurcation.[11] The other important finding was that the nonrigid registration errors were lower than the rigid registration errors for all cases except the external carotid artery in the 3.0 T MR images.

III.D. Comparison of US–MR registration errors at two MR field strengths

The effect of MR field strength on registration error was investigated by performing *paired t-tests* on the nonrigid registration errors of US carotid images with MR images at different field strengths of 1.5 and 3.0 T and the results are shown in Table V. The results obtained did not show statistically significant differences between nonrigid registration accuracy of 3D US images with 1.5 and 3.0 T MR images.

TABLE III. Comparison of the difference in MRE_k (mm) and MRE for rigid and twisting and bending model-based nonrigid registration results with MR images of both field strengths 1.5 and 3.0 T.

Carotid section	Mean difference (mm)		P value		95% CI (mm)	
	1.5 T	3.0 T	1.5 T	3.0 T	1.5 T	3.0 T
Common	0.1[a]	0.2	0.0380	0.1659	0.01–0.2	−0.1–0.6
Internal	0.2[a]	0.4[a]	0.0097	0.0486	0.07–0.4	0.003–0.8
External	0.2	−0.1	0.0995	0.6596	−0.04–0.4	−0.7–0.5
Overall	0.2[a]	0.2[a]	0.0016	0.0178	0.07–0.2	0.04–0.4

[a]Statistically significant (*paired t-test*, $\alpha=0.05$, $1-\beta=0.8$, $P<0.05$) reduction in registration error.

TABLE IV. Maximum registration error ($MAXE_k$) of different carotid sections for both rigid (R) and twisting and bending model-based nonrigid (NR) registration and MR field strengths of 1.5 and 3.0 T.

	Msx. registration error, $MAXE_k$ (mm)											
	1.5 T						3.0 T					
	Common		Internal		External		Common		Internal		External	
	R	NR	R	NR	R	NR	R	NR	R	NR	R	NR
Subject1-L	4.8	5.4	2.0	1.7	2.5	2.2	5.2	3.6	5.6	2.6	3.8	3.7
Subject1-R	5.6	8.2	4.2	3.3	2.2	1.6	4.0	6.4	2.8	1.9	2.2	4.6
Subject2-L	3.5	3.1	3.2	3.0	4.5	5.0	6.5	5.0	3.0	2.7	3.4	4.7
Subject2-R	2.7	3.8	3.1	2.9	2.9	2.4	2.5	3.1	2.1	2.1	2.6	2.3
Subject3-L	5.1	5.0	1.9	1.7	1.3	1.5	5.3	4.4	2.4	2.0	1.5	1.1
Subject3-R	4.5	4.0	3.1	3.1	3.5	3.0	5.6	5.9	1.5	1.4	2.8	3.0
Subject4-L	2.8	4.1	2.8	1.6	3.9	2.5	2.1	2.4	5.3	3.7	2.7	2.4
Subject4-R	4.6	4.4	3.1	2.6	2.1	2.0	4.0	4.0	3.8	3.7	3.8	3.7
Subject5-L	4.0	5.0	3.2	3.3	3.3	3.1	3.5	2.9	2.6	2.7	2.5	2.7
Subject5-R	2.9	3.2	3.8	2.9	1.5	1.3	3.5	2.1	1.9	1.9	1.8	2.4
Subject6-L	6.1	6.0	3.1	2.5	4.9	4.3	4.3	6.8	1.7	1.7	2.6	1.7
Subject6-R	3.1	3.0	3.2	3.4	4.3	4.3	5.0	3.7	2.7	2.0	5.0	4.1

Even though the SNR and CNR are higher for 3.0 T MR images, when other parameters are kept at the same values,[51] the authors did not observe any significant changes in nonrigid registration error after registration with 3D US images.

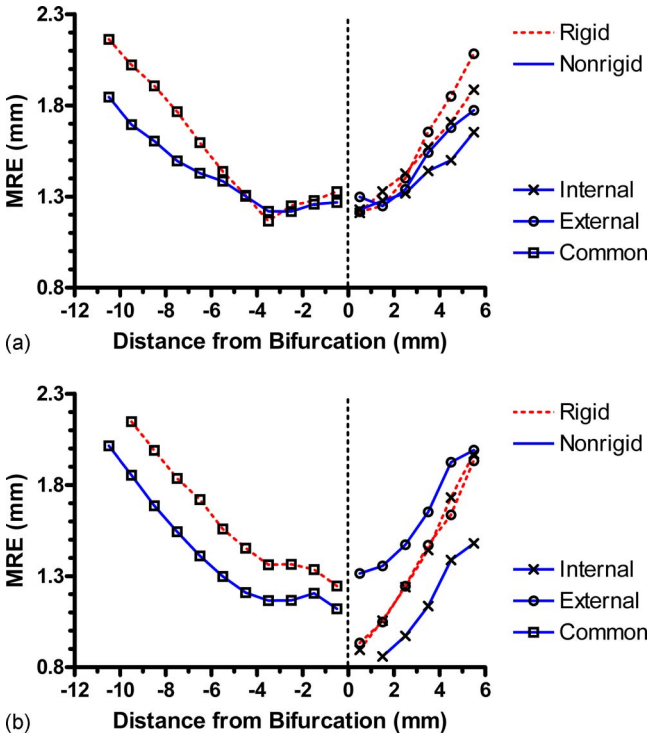

FIG. 7. Average $MRE_{s,k}$ of planes perpendicular to the z axis for intrasubject rigid and twisting and bending model-based nonrigid registration of (a) 3D US with 1.5 T MR and (b) 3D US with 3.0 T MR images of carotid artery, where s is the distance along the z axis from the user-defined carotid bifurcation in the carotid section, k.

IV. DISCUSSION

Atherosclerotic plaques that are vulnerable to disruption, fracture, or fissuring, are at higher risk for embolization, occlusion, and consequent ischemic strokes.[6–8] Noninvasive imaging tools[9–14] that better characterize arterial wall, atherosclerotic plaque structure and composition, and tissue strain and wall shear stress may help to determine the factors that lead to the development of unstable lesions, and identify patients at risk of plaque disruption and stroke. Combining the complementary information provided by 3D MR and US carotid images may lead to a better understanding of the underlying compositional and textural factors that define plaque and wall vulnerability,[15] which may lead to better and more effective stroke prevention strategies and patient management.[32] In addition, it may be advantageous to combine noninvasive MR plaque composition information with 3D US images, since it would provide a tool for *in vivo* validation of US plaque characterization. Although carotid MR imaging allows characterization of plaque composition, it is more expensive and less accessible for use as a monitoring tool, compared to ultrasound. Therefore, development

TABLE V. Comparison of the difference in MRE_k (mm) and MRE for US–MR twisting and bending mode-based nonrigid registration results with MR images of field strengths 1.5 and 3.0 T. There were no statistically significant (*paired t-test*, $\alpha=0.05$, $1-\beta=0.8$, $P<0.05$) changes in registration error.

Carotid section	Mean of MRE difference (mm)	P value	95% confidence interval (mm)
Common	−0.1	0.5636	−0.6–0.3
Internal	0.2	0.3352	−0.3–0.7
External	−0.2	0.6511	−1.0–0.6
Overall	−0.04	0.7764	−0.3–0.3

of noninvasive, less-expensive US imaging tools may be advantageous, since US is already used for measuring carotid stenosis and IMT in clinical settings.

This paper presented an intrasubject nonrigid registration technique to register 3D carotid US and MR images to correct the nonlinear misalignments between them, which is essential for combining the two imaging modalities. A twisting and bending model was used to deform images within the natural movements of the neck. Thus, any unnatural warping of the images during the registration could be avoided. As an added benefit, the number of nonrigid transformation parameters could be limited to six, which is a low number compared to other nonrigid transformations, such as the free form deformation.[55] The twisting and bending model can be changed if a need arises in the future to make it more comprehensive. For example, if the authors change the twisting model from the "cylindrical shaft" to an "elliptical shaft," warping can be introduced to some degree in the z axis, but then the model will have one additional registration parameter. More testing, using either a phantom or different head positions in MR and US image acquisitions, is then necessary to determine if a more complex model would reduce the registration error significantly. The nonrigid registration algorithm presented was tested with 3D US and MR images acquired from subjects with total plaque area >0.5 cm^2. The effects of cardiac pulsation in carotid images, if present, can be a problem in image registration. However, this problem has a very small effect, if any, in patients with carotid atherosclerosis, since the stiffness of the carotid artery increases with progression of the disease,[56] thereby reducing the appearance of cardiac pulsation effects in images.

Since the ground truth was unknown, evaluation of the registration accuracy was challenging. It was very difficult to find a sufficient number of corresponding landmarks in 3D carotid US and MR images to calculate the target registration error. The authors previously used segmented media-adventitia boundary surfaces for evaluating 3D US to US carotid image registration.[36] However, the media-adventitia boundary was not clearly visible in MR images, and therefore the segmented surfaces in US images was expanded by an average adventitia thickness of 0.5 mm (Ref. 53) to calculate the registration errors between adventitia-tissue boundary surfaces. In addition, registration error calculations using segmented vessel boundaries also contain uncertainty due to variability in segmentation. Mean standard error in segmentation has been reported to be about 0.2 mm for similar 3D US images of the carotid arteries.[36]

3D US images with MR images were registered at two field strengths. As shown in Table II, nonrigid registration errors, at both field strengths, were lower in the common and internal carotid arteries than in the external. Similarly, as shown in Fig. 6, nonrigid registration errors were significantly lower than the rigid registration errors in the internal carotid artery, while the change was not statistically significant in the external carotid artery. This was an important observation since the internal carotid artery is more important in managing patients at risk of stroke as it is in the direct path of blood supply to the brain. The diameter of the external carotid is small and sometimes difficult to image with 3D US, making it difficult to register, and optimization process could also be biased toward optimizing the alignment of two larger branches during the registration process. In addition, the external carotid artery is closer to the skin and, therefore, can be moved with respect to the internal carotid in US image acquisition due to the pressure from the probe, and this movement cannot be corrected by the twisting and bending model. Thus, the registration of the external carotid artery was not consistent and therefore improvements were not significant. Since the external carotid artery mainly supplies blood to the external organs in the face, this would not present a significant problem in monitoring carotid plaque. Furthermore, comparing the twisting and bending model-based nonrigid registration technique with other unconstrained nonrigid registration algorithms may be useful to analyze the ability of the technique. However, use of unconstrained nonrigid transformations in registration of 3D US and MR images of the carotid arteries must be avoided to prevent the warping of different plaque components visible in the two modalities.

While nonrigid registration errors in the common carotid artery showed a small but significant improvement over rigid registration for 1.5 T MR, the change in registration error was not significant for 3.0 T MR. The authors did not expect a large difference between rigid and nonrigid registration errors in the common carotid artery as it was anticipated that the most significant nonrigid deformations would be present in the upper part of the carotid arteries since the different head positions deform the upper part of the neck more than the base where the common carotid artery is located. In addition, as shown in Fig. 7, nonrigid registration errors in the internal and common carotid arteries were low near the bifurcation, which is the area usually monitored for carotid plaque.[11] Furthermore, vulnerable plaques may show larger localized changes, mainly ulcerations and fissuring,[57] which are large enough to be detected with registration errors reported in this paper. For an example, Sitzer *et al.*[58] obtained a mean ulceration diameter of 3770 ± 2130 μm (3.7 ± 2.1 mm) for a symptomatic patient population.

Although 3.0 T MR images have a higher SNR and CNR than the 1.5 T images,[51] the authors did not observe statistically significant change in registration errors between them, as shown in Table V. An important factor may be due to the use of MI as the image similarity measure, which has been shown to be robust in the presence of noise and intensity value variations.[37,38,43] It may also be beneficial to study the differences in segmentations in 1.5 and 3.0 T MR images after aligning them by rigid registration. However, a number of previous studies for other applications has not shown significant differences in physical measurements and diagnostic accuracy.[59,60]

The nonrigid registration technique presented in this paper required some user interaction in preprocessing and initialization. In preprocessing, a user-selected ROI must be defined but the effect of variability in ROI selection would have a minimal effect on the final results due to the use of

NMI as image similarity measure. NMI is insensitive to the changes of overlap of ROI defined in the two images.[61] In addition, the user must select four points on each of the two images for initializing the registration. One point each in each image is used to identify the carotid bifurcation to be used to calculate both initial transformations and rotations and it has been shown that the carotid bifurcation can be located in 3D US images with a standard deviation of 0.56 mm.[27] The other three points together with the bifurcation are used to calculate the initial rotation. Since this initial coarse alignment was allowed to change during the registration, it was assumed that the variability in point selections was relatively insignificant to the final registration results.

Processing time of 10–40 min for registration of one pair of images can be considered higher than normal for a registration technique with only 12 parameters (6 rigid and 6 nonrigid). The authors have not optimized the program yet and have used a user interface implemented in Python programming language. Therefore, speed may be improved by optimizing the program and implementing the whole program in C++. In addition, large 3D US images (about 400 $\times 350 \times 750$ voxels) could have contributed to the high processing time. Thus, the speed can be improved by downsampling the 3D US images, but more tests would be required to find a balance between processing time and registration accuracy.

Speckle in US images provides useful information to the radiologist, but together with shadowing and other artifacts, makes registration prone to errors. The authors minimized the effect of this problem by using MI and nongradient-based Powell optimizer. Tissue mimicking flow artifacts of MR images[62] might create some problems with the registration process and more research is needed to find ways to overcome these limitations. Effects on the registration process by other anatomical structures in the carotid images were reduced by masking out the area outside the carotid artery and its surrounding. Although effects due to the presence of cardiac pulsation in carotid images were small for patients with stiff arterial wall,[63] they may be further minimized by using cardiac gating image acquisitions.

V. CONCLUSION

A nonrigid registration technique to register intrasubject 3D US and MR carotid images has been developed using a twisting and bending model, normalized mutual information, and Powell optimization method. The technique was tested with 3D US and corresponding 1.5 and 3.0 T MR images acquired on the same day and overall errors of 1.4 ± 0.3 mm for 1.5 T and 1.5 ± 0.4 mm for 3.0 T were obtained. However, these values also include the uncertainties from expansion of media-adventitia boundary in the US images to establish the adventitia-tissue boundary and variability in segmentation. Therefore, the actual registration errors may be less than the reported values. More important, lower registration errors were obtained in the internal and common carotid arteries, especially close to the carotid bifurcation, where most of the plaque accumulates due to the arterial remodeling in the presence of atherosclerosis.

ACKNOWLEDGMENTS

The authors wish to thank Trevor Wade and Adam Krasinski for carotid artery segmentations. This work has been supported by the Canadian Institutes for Health Research (CIHR), The Richard Ivey Foundation, and Ontario Graduate Scholarship program. A.F. holds a Canada Research Chair and acknowledges The Canada Research Chair Program.

[a]Electronic mail: nnanayak@uwo.ca
[b]Electronic mail: afenster@imaging.robarts.ca

[1]*Stroke Statistics*, The Heart and Stroke Foundation of Canada, Ottawa, Ontario, Canada (2008). URL: http://www.heartandstroke.ca.
[2]*Stroke Facts and Statistics*, Centers for Disease Control and Prevention, Department of Health and Human Services, Atlanta, GA (2007). URL: http://www.cdc.gov/stroke.
[3]B. M. Eicke, J. von Lorentz, and W. Paulus, "Embolus detection in different degrees of carotid disease," Neurol. Res. **17**, 181–184 (1995).
[4]F. Fabris, M. Zanocchi, M. Bo, G. Fonte, L. Poli, I. Bergoglio, E. Ferrario, and L. Pernigotti, "Carotid plaque, aging, and risk factors. A study of 457 subjects," Stroke **25**, 1133–1140 (1994).
[5]Executive Committee for the Asymptomatic Carotid Atherosclerosis Study, "Endarterectomy for asymptomatic carotid artery stenosis," JAMA, J. Am. Med. Assoc. **273**, 1421–1428 (1995).
[6]E. Falk, "Why do plaques rupture¿" Circulation **86**, III30–42 (1992).
[7]M. J. Davies, "Pathology of arterial thrombosis," Br. Med. Bull. **50**, 789–802 (1994).
[8]J. Golledge, R. M. Greenhalgh, and A. H. Davies, "The symptomatic carotid plaque," Stroke **31**, 774–781 (2000).
[9]J. F. Toussaint, G. M. LaMuraglia, J. F. Southern, V. Fuster, and H. L. Kantor, "Magnetic resonance images lipid, fibrous, calcified, hemorrhagic, and thrombotic components of human atherosclerosis in vivo," Circulation **94**, 932–938 (1996).
[10]G. A. Lammie, J. Wardlaw, P. Allan, C. V. Ruckley, R. Peek, and D. F. Signorini, "What pathological components indicate carotid atheroma activity and can these be identified reliably using ultrasound¿" Eur. J. Ultrasound **11**, 77–86 (2000).
[11]C. D. Ainsworth, C. C. Blake, A. Tamayo, V. Beletsky, A. Fenster, and J. D. Spence, "3D ultrasound measurement of change in carotid plaque volume: A tool for rapid evaluation of new therapies," Stroke **36**, 1904–1909 (2005).
[12]B. K. Lal, R. W. Hobson II, M. Hameed, P. J. Pappas, F. T. Padberg, Jr., Z. Jamil, and W. N. Duran, "Noninvasive identification of the unstable carotid plaque," Ann. Vasc. Surg. **20**, 167–174 (2006).
[13]T. Saam, T. S. Hatsukami, N. Takaya, B. Chu, H. Underhill, W. S. Kerwin, J. Cai, M. S. Ferguson, and C. Yuan, "The vulnerable, or high-risk, atherosclerotic plaque: Noninvasive MR imaging for characterization and assessment," Radiology **244**, 64–77 (2007).
[14]D. N. Ku, D. P. Giddens, C. K. Zarins, and S. Glagov, "Pulsatile flow and atherosclerosis in the human carotid bifurcation. Positive correlation between plaque location and low oscillating shear stress," Arteriosclerosis (Dallas) **5**, 293–302 (1985).
[15]R. C. Chan, S. Sokka, D. Hinton, S. Houser, R. Manzke, A. Hanekamp, V. Y. Reddy, M. R. Kaazempur-Mofrad, and V. Rasche, "Non-rigid registration for fusion of carotid vascular ultrasound and MRI volumetric datasets," in *Medical Imaging 2006: Image Processing* (SPIE, 2006), Vol. 6144, pp. 61442E-1–8.
[16]C. Yuan *et al.*, "MRI of atherosclerosis in clinical trials," NMR Biomed. **19**, 636–654 (2006).
[17]C. Yuan, K. W. Beach, L. H. Smith, Jr., and T. S. Hatsukami, "Measurement of atherosclerotic carotid plaque size in vivo using high resolution magnetic resonance imaging," Circulation **98**, 2666–2671 (1998).
[18]J. Cai, T. S. Hatsukami, M. S. Ferguson, W. S. Kerwin, T. Saam, B. Chu, N. Takaya, N. L. Polissar, and C. Yuan, "In vivo quantitative measurement of intact fibrous cap and lipid-rich necrotic core size in atherosclerotic carotid plaque: Comparison of high-resolution, contrast-enhanced magnetic resonance imaging and histology," Circulation **112**, 3437–3444 (2005).
[19]T. S. Hatsukami, R. Ross, N. L. Polissar, and C. Yuan, "Visualization of fibrous cap thickness and rupture in human atherosclerotic carotid plaque in vivo with high-resolution magnetic resonance imaging," Circulation

102, 959–964 (2000).
[20]Z. A. Fayad and V. Fuster, "Clinical imaging of the high-risk or vulnerable atherosclerotic plaque," Circ. Res. **89**, 305–316 (2001).
[21]E. K. Yucel, C. M. Anderson, R. R. Edelman, T. M. Grist, R. A. Baum, W. J. Manning, A. Culebras, and W. Pearce, "AHA scientific statement. Magnetic resonance angiography: Update on applications for extracranial arteries," Circulation **100**, 2284–2301 (1999).
[22]J. D. Spence, "Technology Insight: Ultrasound measurement of carotid plaque—Patient management, genetic research, and therapy evaluation," Nat. Clin. Pract. Neurol. **2**, 611–619 (2006).
[23]H. J. M. Barnett, D. W. Taylor, M. Eliasziw, A. J. Fox, G. G. Ferguson, R. B. Haynes, R. N. Rankin, G. P. Clagett, V. C. Hachinski, D. L. Sackett *et al.*, "Benefit of carotid endarterectomy in patients with symptomatic moderate or severe stenosis," N. Engl. J. Med. **339**, 1415–1425 (1998).
[24]M. G. Hunink, J. F. Polak, M. M. Barlan, and D. H. O'Leary, "Detection and quantification of carotid artery stenosis: Efficacy of various Doppler velocity parameters," AJR, Am. J. Roentgenol. **160**, 619–625 (1993).
[25]R. T. Hurst, D. W. Ng, C. Kendall, and B. Khandheria, "Clinical use of carotid intima-media thickness: Review of the literature," J. Am. Soc. Echocardiogr **20**, 907–914 (2007).
[26]J. J. Cao, C. Thach, T. A. Manolio, B. M. Psaty, L. H. Kuller, P. H. Chaves, J. F. Polak, K. Sutton-Tyrrell, D. M. Herrington, T. R. Price, and M. Cushman, "C-reactive protein, carotid intima-media thickness, and incidence of ischemic stroke in the elderly: The cardiovascular health study," Circulation **108**, 166–170 (2003).
[27]A. Landry, C. Ainsworth, C. Blake, J. D. Spence, and A. Fenster, "Manual planimetric measurement of carotid plaque volume using three-dimensional ultrasound imaging," Med. Phys. **34**, 1496–1505 (2007).
[28]A. Landry, J. D. Spence, and A. Fenster, "Measurement of carotid plaque volume by 3-dimensional ultrasound," Stroke **35**, 864–869 (2004).
[29]J. D. Spence, M. Eliasziw, M. DiCicco, D. G. Hackam, R. Galil, and T. Lohmann, "Carotid plaque area: A tool for targeting and evaluating vascular preventive therapy," Stroke **33**, 2916–2922 (2002).
[30]M. Egger, J. D. Spence, A. Fenster, and G. Parraga, "Validation of 3D ultrasound vessel wall volume: An imaging phenotype of carotid atherosclerosis," Ultrasound Med. Biol. **33**, 905–914 (2007).
[31]M. Egger, B. Chiu, J. D. Spence, A. Fenster, and G. Parraga, "Mapping spatial and temporal changes in carotid atherosclerosis from three-dimensional ultrasound images," Ultrasound Med. Biol. **34**, 64–72 (2008).
[32]M. Fisher, A. Paganini-Hill, A. Martin, M. Cosgrove, J. F. Toole, H. J. Barnett, and J. Norris, "Carotid plaque pathology: Thrombosis, ulceration, and stroke pathogenesis," Stroke **36**, 253–257 (2005).
[33]F. P. Glor, B. Ariff, L. A. Crowe, A. D. Hughes, P. L. Cheong, S. A. Thom, P. R. Verdonck, D. N. Firmin, D. C. Barratt, and X. Y. Xu, "Carotid geometry reconstruction: A comparison between MRI and ultrasound," Med. Phys. **30**, 3251–3261 (2003).
[34]P. J. Slomka, J. Mandel, D. Downey, and A. Fenster, "Evaluation of voxel-based registration of 3-D power Doppler ultrasound and 3-D magnetic resonance angiographic images of carotid arteries," Ultrasound Med. Biol. **27**, 945–955 (2001).
[35]B. Fei, S. Zhang, O. Savado, J. Suri, J. S. Lewin, and D. L. Wilson, "Three-dimensional automatic volume registration of carotid MR images," in *Proceedings of the 25th Annual International Conference* (IEEE Engineering in Medicine and Biology Society, 2003), Vol. 1, pp.646–648.
[36]N. D. Nanayakkara, B. Chiu, A. Samani, J. D. Spence, J. Samarabandu, and A. Fenster, "A 'twisting and bending' model-based nonrigid image registration technique for 3D ultrasound carotid images," IEEE Trans. Med. Imag., in press, published online (Digital Object Identifier: 10.1109/TMI.2008.918326).
[37]W. M. Wells, P. Viola, H. Atsumi, S. Nakajima, and R. Kikinis, "Multi-model volume registration by maximization of mutual information," Med. Image Anal. **1**, 35–51 (1996).
[38]F. Maes, A. Collignon, D. Vandermeulen, G. Marchal, and P. Suetens, "Multimodality image registration by maximization of mutual information," IEEE Trans. Med. Imaging **16**, 187–198 (1997).
[39]J. P. W. Pluim, J. B. A. Maintz, and M. A. Viergever, "Mutual-information-based registration of medical images: A survey," IEEE Trans. Med. Imaging **22**, 986–1004 (2003).
[40]D. H. Ballard and C. M. Brown, *Computer Vision* (Prentice-Hall, Englewood Cliffs, NJ, 1982).
[41]F. P. Beer, E. R. Johnston, and J. T. DeWolf, *Mechanics of Materials* (McGraw-Hill Higher Education, Boston, 2006).
[42]C. Studholme, D. L. G. Hill, and D. J. Hawkes, "An overlap invariant entropy measure of 3D medical image alignment," Pattern Recogn. **32**, 71–86 (1999).
[43]D. L. G. Hill, P. G. Batchelor, M. Holden, and D. J. Hawkes, "Medical image registration," Phys. Med. Biol. **46**, R1–R45 (2001).
[44]D. Mattes, D. R. Haynor, H. Vesselle, T. K. Lewellyn, and W. Eubank, "Nonrigid multimodality image registration," in *Medical Imaging 2001: Image Processing* (SPIE, 2001), Vol. 4322, pp. 1609–1620.
[45]D. Mattes, D. R. Haynor, H. Vesselle, T. K. Lewellen, and W. Eubank, "PET-CT image registration in the chest using free-form deformations," IEEE Trans. Med. Imaging **22**, 120–128 (2003).
[46]W. H. Press, B. P. Flannery, S. A. Teukolsky, and W. T. Vetterling, *Numerical Recipes in C: The Art of Scientific Computing* (Cambridge University Press, New York, 1988).
[47]J. Tsao, "Interpolation artifacts in multimodality image registration based on maximization of mutual information," IEEE Trans. Med. Imaging **22**, 854–864 (2003).
[48]"The insight segmentation and registration toolkit," URL: www.itk.org.
[49]W. L. Smith and A. Fenster, "Optimum scan spacing for three-dimensional ultrasound by speckle statistics," Ultrasound Med. Biol. **26**, 551–562 (2000).
[50]M. Egger, C. Blake, A. Vidal, J. Kost, J. Spence, B. Rutt, A. Fenster, A. House, and G. Parraga, "Po-Thur Eve General-24: Non-invasive imaging phenotypes of carotid atherosclerosis in subjects: MRI, B-mode and 3D ultrasound measurements," Med. Phys. **33**, 2664–2664 (2006).
[51]V. L. Yarnykh, M. Terashima, C. E. Hayes, A. Shimakawa, N. Takaya, P. K. Nguyen, J. H. Brittain, M. V. McConnell, and C. Yuan, "Multicontrast black-blood MRI of carotid arteries: Comparison between 1.5 and 3 Tesla magnetic field strengths," J. Magn. Reson Imaging **23**, 691–698 (2006).
[52]H. R. Underhill, W. S. Kerwin, T. S. Hatsukami, and C. Yuan, "Automated measurement of mean wall thickness in the common carotid artery by MRI: A comparison to intima-media thickness by B-mode ultrasound," J. Magn. Reson Imaging **24**, 379–387 (2006).
[53]M. Wong, J. Edelstein, J. Wollman, and M. G. Bond, "Ultrasonic-pathological comparison of the human arterial wall. Verification of intima-media thickness," Arterioscler. Thromb. **13**, 482–486 (1993).
[54]A. N. Kolmogorov, A. A. Petrov, and Y. M. Smirnov, "A formula of Gauss from the method of least squares," Izv. Akad. Nauk SSSR, Ser. Mat. **11**, 561–566 (1947).
[55]D. Rueckert, L. I. Sonoda, C. Hayes, D. L. Hill, M. O. Leach, and D. J. Hawkes, "Nonrigid registration using free-form deformations: Application to breast MR images," IEEE Trans. Med. Imaging **18**, 712–721 (1999).
[56]R. S. Reneman, T. van Merode, P. Hick, A. M. Muytjens, and A. P. Hoeks, "Age-related changes in carotid artery wall properties in men," Ultrasound Med. Biol. **12**, 465–471 (1986).
[57]A. Fenster, C. Blake, I. Gyacskov, A. Landry, and J. D. Spence, "3D ultrasound analysis of carotid plaque volume and surface morphology," Ultrasonics **44**, e153–e157 (2006).
[58]M. Sitzer, W. Muller, M. Siebler, W. Hort, H. W. Kniemeyer, L. Jancke, and H. Steinmetz, "Plaque ulceration and lumen thrombus are the main sources of cerebral microemboli in high-grade internal carotid artery stenosis," Stroke **26**, 1231–1233 (1995).
[59]T. Sommer, M. Hackenbroch, U. Hofer, A. Schmiedel, W. A. Willinek, S. Flacke, J. Gieseke, F. Trber, R. Fimmers, H. Litt, and H. Schild, "Coronary MR angiography at 3.0 T versus that at 1.5 T: Initial results in patients suspected of having coronary artery disease," Radiology **234**, 718–725 (2005).
[60]P. R. Kornaat, S. B. Reeder, S. Koo, J. H. Brittain, H. Yu, T. P. Andriacchi, and G. E. Gold, "MR imaging of articular cartilage at 1.5 T and 3.0 T: Comparison of SPGR and SSFP sequences," Osteoarthritis Cartilage **13**, 338–344 (2005).
[61]D. L. G. Hill and P. Batchelor, "Registration methodology: Concepts and algorithms," in *Medical Image Registration* (CRC Press, Boca Raton, FL, 2001), pp. 39–70.
[62]D. A. Steinman and B. K. Rutt, "On the nature and reduction of plaque-mimicking flow artifacts in black blood MRI of the carotid bifurcation," Magn. Reson. Med. **39**, 635–641 (1998).
[63]A. Delcker and C. Tegeler, "Influence of ecg-triggered data acquisition on reliability for carotid plaque volume measurements with a magnetic sensor three-dimensional ultrasound system," Ultrasound Med. Biol. **24**, 601–605 (1998).